Journal of Mathematical Imaging and Vision
https://doi.org/10.1007/s10851-020-00953-w

Optimum Cuts in Graphs by General Fuzzy Connectedness with Local Band Constraints

Caio de Moraes Braz[1] · Paulo A. V. Miranda[1] · Krzysztof Chris Ciesielski[2] · Fábio A. M. Cappabianco[3]

Received: 9 July 2019 / Accepted: 8 March 2020

Abstract
The goal of this work is to describe an efficient algorithm for finding a binary segmentation of an image such that the indicated object satisfies a novel high-level prior, called local band, LB, constraint; the returned segmentation is optimal, with respect to an appropriate graph-cut measure, among all segmentations satisfying the given LB constraint. The new algorithm has two stages: expanding the number of edges of a standard edge-weighted graph of an image; applying to this new weighted graph an algorithm known as an oriented image foresting transform, OIFT. In our theoretical investigation, we prove that OIFT algorithm belongs to a class of general fuzzy connectedness algorithms and so has several good theoretical properties, like robustness for seed placement. The extension of the graph constructed in the first stage ensures, as we prove, that the resulted object indeed satisfies the given LB constraint. We also notice that this graph construction is flexible enough to allow combining it with other high-level constraints. Finally, we experimentally demonstrate that the LB constraint gives competitive results as compared to geodesic star convexity, boundary band, and hedgehog shape prior, all implemented within OIFT framework and applied to various scenarios involving natural and medical images.

Keywords Boundary band constraint · Hedgehog shape prior · Image foresting transform · Graph-cut segmentation

1 Introduction

Image segmentation is one of the most fundamental and challenging problems in image processing and computer vision. In many scenarios, the high-level, application domain-specific knowledge of the user is often required in the segmentation process because of the presence of heterogeneous backgrounds, objects with ill-defined borders, field inhomogeneity, noise, artifacts, partial volume effects, and their interplay [25]. It may be thought of as consisting of two related processes—object recognition and delineation [16]. Recognition is the task of determining an object's approximate whereabouts in the image. Delineation completes segmentation by defining the exact spatial extent of that object. In this work, we are interested in solving the delineation problem by fast methods to efficiently deal with large amounts of data, but which must also be versatile enough to support the inclusion of high-level constraints from prior object knowledge.

The segmentation problem can be interpreted as a graph partition problem subject to hard constraints, such as seed pixels selected in the image domain for object recognition, by modeling neighborhood relations of picture elements from digital images. Examples of seed-based methods are watershed [11,12], random walks [18], fuzzy connectedness [7], graph cuts (GC) [3], grow cut [24], minimum barrier distance [10], and image foresting transform (IFT) [8,15]. Some

Thanks to CNPq (313554/2018-8, 486988/2013-9, FINEP 1266/13), FAPESP (2014/12236-1, 2016/21591-5), Coordenação de Aperfeiçoamento de Pessoal de Nível Superior - Brasil (CAPES) - Finance Code 001, and NAP eScience - PRP - USP for funding.

✉ Paulo A. V. Miranda
pmiranda@ime.usp.br

Caio de Moraes Braz
caiobraz@ime.usp.br

Krzysztof Chris Ciesielski
Krzysztof.Ciesielski@mail.wvu.edu

Fábio A. M. Cappabianco
cappabianco@unifesp.br

[1] Institute of Mathematics and Statistics, University of São Paulo, São Paulo, SP CEP 05508-090, Brazil

[2] Department of Mathematics, West Virginia University, Morgantown, USA

[3] Instituto de Ciência e Tecnologia, São José dos Campos, SP, Brazil

Published online: 27 March 2020

methods, including the min-cut/max-flow algorithm, can provide global optimal solutions according to a graph-cut measure in graphs and can be described in a unified manner according to a common framework, which we refer to as generalized graph cut (GGC) [5]. (See also [6].)

Oriented image foresting transform (OIFT) [30] and *oriented relative fuzzy connectedness* (ORFC) [2] are extensions of some GGC methods for directed weighted graphs, which have lower computational complexity compared to the min-cut/max-flow algorithm [3]. Also, as we will show, OIFT belongs to a class of general fuzzy connectedness algorithms described in [9]. OIFT is a flexible method, which has been extended to support the processing of global object properties, such as connectedness [26,27], shape constraints [13,29], boundary polarity [2,28], and hierarchical constraints [22]. These high-level priors are potentially useful for object segmentation, allowing the customization of the segmentation to a given target object. Shape constraints can be used to eliminate undesirable intricate forms, improving the segmentation of objects with more regular contour. Some shape constraints demand more sophisticated algorithms, such as the *boundary band constraint* (BB) [13]. The OIFT with the BB constraint allows the segmentation to follow a pre-established template of shapes, with variances within a range of permitted deformations around an arbitrary scale, while other approaches handle scale inefficiently based on brute force, by computing the graph cut for each level of a Gaussian pyramid [17].

In this work, we propose a novel shape constraint, named *local band constraint* (LB), to be used for object segmentation in the generalized GC framework which, in its limit case, is strongly related to the boundary band constraint [13]. The LB constraint demonstrates competitive results with higher accuracy when compared to BB, hedgehog [20,21], and geodesic star convexity [19] in various scenarios. It can also be easily combined with other high-level priors already supported by OIFT, considerably advancing the targeted segmentation [23]. For the sake of simplicity, we are only presenting its results for binary segmentation. But the LB constraint can, in theory, be incorporated into the layers of a hierarchical layered digraph [22] to perform also multi-object segmentation.

The next section gives the required background on image graphs and GGC. In Sects. 3 and 4 we show, respectively, that OIFT can be seen as belonging to the generalized graph cut and the general fuzzy connectedness frameworks. This is the new material that has not been presented in the conference version of the paper [14]. The proposed local band constraint is presented in Sect. 5. In Sect. 6, we experimentally evaluate LB, comparing it to previous graph-based works on shape constraints. Our conclusions are stated in Sect. 7.

2 Background

An image can be interpreted as a directed graph (digraph) $G = \langle \mathcal{N}, \mathcal{A} \rangle$ whose nodes/vertices are the image pixels in its image domain $\mathcal{N} \subset \mathbb{Z}^n$ and whose arcs/edges, elements of $\mathcal{A}$, are the ordered pixel pairs $\langle s, t \rangle$ of vertices that are adjacent, that is, spatially close (e.g., 4-neighborhood, or 8-neighborhood, in the case of 2D images). We write $t \in \mathcal{A}(s)$ or $\langle s, t \rangle \in \mathcal{A}$ to indicate that t is adjacent to s. We will usually assume also that our image graph G is edge-weighted, that is, that each arc $\langle s, t \rangle \in \mathcal{A}$ has a fixed weight $\omega(s, t) \in [-\infty, \infty]$ (often $\omega(s, t) = \|\mathcal{I}(t) - \mathcal{I}(s)\|$ for an image with values given by $\mathcal{I}(t)$). An edge-weighted digraph will be denoted as $G = \langle \mathcal{N}, \mathcal{A}, \omega \rangle$. A digraph G is symmetric if, for all $\langle s, t \rangle \in \mathcal{A}$, the pair $\langle t, s \rangle$ is also an arc of G. Note that in the symmetric graphs we can still have $\omega(s, t) \neq \omega(t, s)$. In this work, all considered graphs are symmetric and connected.

A *path* (*in* G) of length $\ell \geq 0$ is any sequence $p_v = \langle v_0, \ldots, v_\ell \rangle$ of vertices, with *terminus* $v = v_\ell$, such that $\langle v_j, v_{j+1} \rangle \in \mathcal{A}$ for any $j < \ell$; it is *from* $\mathcal{S} \subset \mathcal{N}$ *to* $v \in \mathcal{N}$ when $v_0 \in \mathcal{S}$ and $v_\ell = v$; if $\langle v, w \rangle \in \mathcal{A}$, then $p_v \hat{} w$ denotes the path $\langle v_0, \ldots, v_\ell, w \rangle$. Let Π_G be the family of all paths in G and consider a path-cost function $\psi : \Pi_G \to [-\infty, \infty]$.

Image segmentation can be formulated as a graph partition problem subject to hard constraints. In the case of binary segmentation (object/background), we consider two non-empty disjoint seed sets $\mathcal{S}_1$ and $\mathcal{S}_0$ containing pixels selected inside the object $\mathcal{O}$ and in its exterior, respectively. A label, $L(t) = 1$ for all $t \in \mathcal{S}_1$ and $L(t) = 0$ for all $t \in \mathcal{S}_0$, is propagated to all unlabeled pixels during the execution of seed-based segmentation algorithms, see, e.g., [30]. For a label map $L : \mathcal{N} \to \{0, 1\}$ the object $\mathcal{O}$ identified with it is defined as the set $L^{-1}(1)$, where $L^{-1}(i) := \{t \in \mathcal{N} : L(t) = i\}$.

In what follows, the key tool for finding optimized label maps L is OIFT Algorithm 1, which comes from [28,30]. The OIFT will be a part of our novel algorithm. The map L it returns constitutes a global optimum solution that maximizes the following graph-cut measure

$$\varepsilon_{\min}(L) := \min\{\omega(s, t) : \langle s, t \rangle \in \mathcal{A} \;\&\; L(s) > L(t)\} \qquad (1)$$

subject to the seed constraints [28,30]:

Proposition 1 (Mansilla and Miranda 2013) *Let* $G = \langle \mathcal{N}, \mathcal{A}, \omega \rangle$ *be a symmetric edge-weighted image digraph. Let* L *be a segmentation returned by Algorithm 1 applied to* G *and non-empty disjoint seed sets* $\mathcal{S}_0$ *and* $\mathcal{S}_1$*. Then* L *satisfies the seed constraints and maximizes the energy* $\varepsilon_{\min}$*, given by* (1)*, among all segmentations satisfying these constraints.*

Notice that in line 12 of OIFT Algorithm 1 the weight $\omega(t, s)$ of the reversed parallel arc $\langle t, s \rangle$ is used (rather than that of chosen $\langle s, t \rangle \in \mathcal{A}$). That is why a symmetric digraph is required.

Algorithm 1 – SEGMENTATION ALGORITHM OIFT

INPUT: Symmetric edge-weighted image digraph $\langle \mathcal{N}, \mathcal{A}, \omega \rangle$ and non-empty disjoint seed sets $\mathcal{S}_0$ and $\mathcal{S}_1$.
OUTPUT: The label map $L : \mathcal{N} \to \{0, 1\}$.
AUXILIARY: An initially empty set Q, variable tmp, and an array of status $S : \mathcal{N} \to \{0, 1\}$, where $S(t) = 1$ for processed nodes and $S(t) = 0$ for unprocessed nodes. The value $V(t)$ represents a potential penalty that a change of $L(t)$ would contribute to $\varepsilon_{\min}(L)$.

1. **For each** $t \in \mathcal{N}$, **do**
2. *Set* $S(t) \leftarrow 0$ *and* $V(t) \leftarrow \infty$;
3. **If** $t \in \mathcal{S}_0$, **then**
4. $V(t) \leftarrow -\infty$, $L(t) \leftarrow 0$, *and insert* t *in* Q;
5. **If** $t \in \mathcal{S}_1$ **then**
6. $V(t) \leftarrow -\infty$, $L(t) \leftarrow 1$, *and insert* t *in* Q.
7. **While** $Q \neq \emptyset$ **do**
8. *Remove* s *from* Q *such that* $V(s)$ *is minimum.*
9. *Set* $S(s) \leftarrow 1$.
10. **For each** $\langle s, t \rangle \in \mathcal{A}$ *such that* $S(t) = 0$ **do**
11. **If** $L(s) = 1$, **then** $tmp \leftarrow \omega(s, t)$.
12. **Else** $tmp \leftarrow \omega(t, s)$;
13. **If** $tmp < V(t)$, **then**
14. *Set* $V(t) \leftarrow tmp$ *and* $L(t) \leftarrow L(s)$.
15. **If** $t \notin Q$, **then** *insert* t *in* Q.
16. *Return* L.

The OIFT algorithm is based on a label propagation from the seeds, such that the growing object avoids traversing high-weighted arcs. The node propagation priority is governed by map V, such that the lower the value $V(t)$ the higher its priority. Initially, seeds are initialized with maximum priority $V(t) = -\infty$ on lines 1–6. During propagation (lines 7–15), nodes with $S(t) = 1$ reach their final label assignment and can no longer be modified. Figure 1a–g shows a step-by-step illustration of the execution of Algorithm 1, and its resulting optimal cut is shown in Fig. 1h.

Regarding the computational complexity of Algorithm 1, the nodes in Q should be organized according to an appropriate data structure of a priority queue in order to support the efficient removal of its element with minimum value of $V(t)$ from line 8. If a binary heap is used for Q, then Algorithm 1 can be implemented in $O((m + n) \log n)$, where $n = |\mathcal{N}|$, $m = |\mathcal{A}|$, and $|\cdot|$ denotes the set cardinality. Note that in this case the position of a node t in the binary heap must be updated whenever we change its value of $V(t)$ in line 14. This computational complexity can be improved to $O(m+n \times K)$, when the weights are integers in a small interval of size K, by using bucket sorting. Note also that the special configuration of infinite-weight arcs is not a problem as they can be assigned to a special bucket.

OIFT Algorithm 1 can also be adapted for multi-object segmentation by computing a related variant in a hierarchical layered digraph [22].

In the next two sections, we will show that OIFT belongs to two general algorithmic frameworks: GGC and GFC.

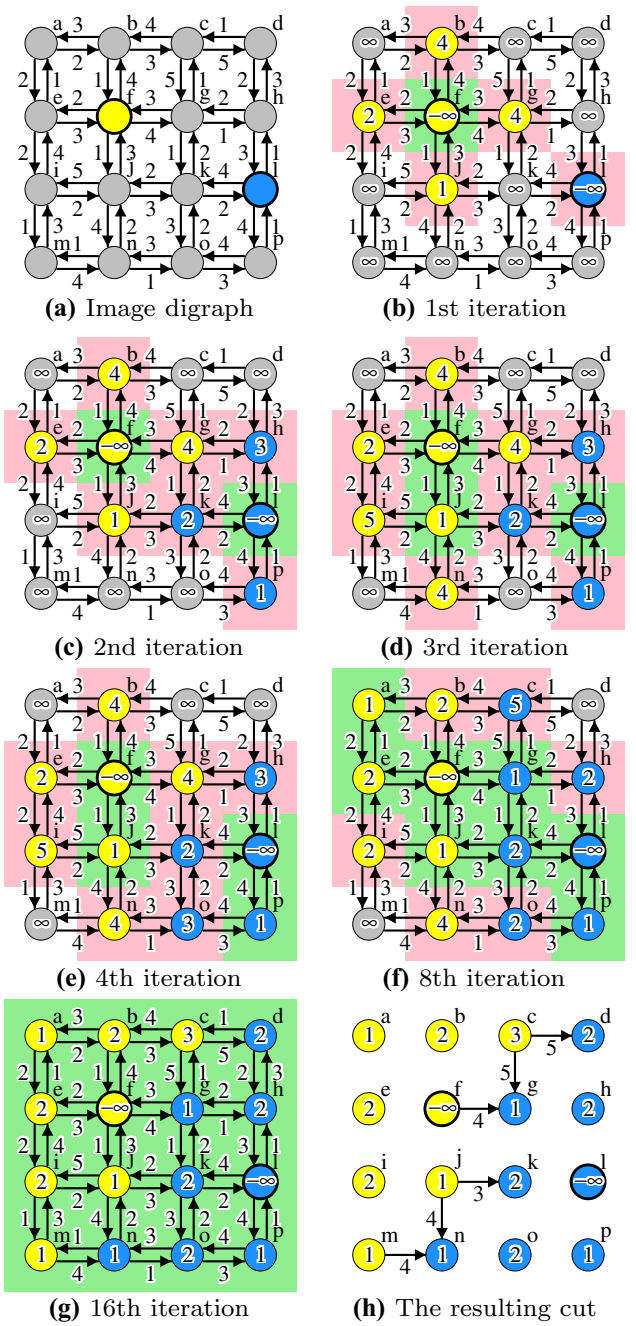

Fig. 1 An example of the step-by-step execution of Algorithm 1. **a** An image digraph with 4-neighborhood and seeds $\mathcal{S}_0 = \{l\}$ (in blue) and $\mathcal{S}_1 = \{f\}$ (in yellow). **b** The label propagation after one iteration of the main loop (lines 7–15), where the node colors blue and yellow indicate the labels $L(t) = 0$ and $L(t) = 1$, respectively, a pink-colored background indicates pixels in Q, while a green background indicates processed nodes in $\{t \in \mathcal{N} : S(t) = 1\}$. The values $V(t)$ are indicated inside the nodes. **c–g** The results of the next iterations. **h** The arcs in the resulting optimal cut $\{\langle s, t \rangle \in \mathcal{A} : L(s) > L(t)\}$ with $\varepsilon_{\min}(L) = \omega(j, k) = 3$ (Color figure online)

Algorithm 2 – OIFT* ALGORITHM

INPUT: Image graph $\langle \mathcal{N}, \mathcal{A} \rangle$, weight maps w_0 and w_1, seed sets $\mathcal{S}_0$ and $\mathcal{S}_1$.
OUTPUT: The label map $L: \mathcal{N} \to \{0, 1\}$ and an array $\pi[\,]$ such that if $S(t) = 1$, then $\pi[t]$ is a path from $\mathcal{S}_{L(t)}$ to t.
AUXILIARY: An initially empty set Q, variable tmp, the cost function $V: \mathcal{N} \to [-\infty, \infty]$, and a status function $S: \mathcal{N} \to \{0, 1\}$, where $S(t) = 1$ for processed nodes and $S(t) = 0$ for unprocessed nodes.

1. **For each** $t \in \mathcal{N}$, **do**
2. Set $S(t) \leftarrow 0$, $V(t) \leftarrow -\infty$, *and* $\pi[t] \leftarrow \langle t \rangle$;
3. **If** $t \in \mathcal{S}_0$, **then**
4. $V(t) \leftarrow \infty$, $L(t) \leftarrow 0$, *and insert* t *in* Q;
5. **If** $t \in \mathcal{S}_1$ **then**
6. $V(t) \leftarrow \infty$, $L(t) \leftarrow 1$, *and insert* t *in* Q.
7. **While** $Q \neq \emptyset$ **do**
8. *Remove* s *from* Q *with* $V(s) \geq V(t)$ *for all* $t \in Q$;
9. Set $S(s) \leftarrow 1$;
10. **For each** $\langle s, t \rangle \in \mathcal{A}$ *such that* $S(t) = 0$ **do**
11. $tmp \leftarrow w_{L(s)}(s, t)$;
12. **If** $tmp > V(t)$ **then**
13. Set $V(t) \leftarrow tmp$, $\pi[t] \leftarrow \pi[s]\hat{}t$ *and* $L(t) \leftarrow L(s)$.
14. **If** $t \notin Q$ **then** *insert* t *in* Q.

3 OIFT as a Generalized Graph-Cut Algorithm

The biggest difference between OIFT Algorithm 1 and the algorithms in the GGC framework [5] is that in the former case we *maximize* the energy function, while in the latter case we *minimize* its analog. To represent OIFT as a minimization problem it is enough to reverse in it all inequalities, exchange terms "∞" with "$-\infty$" and "minimum" with "maximum," and replace the weight function $\omega(s, t)$ with a function[1] $\bar{\omega}(s, t) := e^{-\omega(s,t)}$. Specifically, we represent OIFT as OIFT* Algorithm 2, for which we have the following result.

Proposition 2 *OIFT Algorithm 1 applied to* $\langle \mathcal{N}, \mathcal{A}, \omega \rangle$ *and the seed sets* $\mathcal{S}_0$ *and* $\mathcal{S}_1$ *can return the label map* L *if, and only if,* L *can be returned by OIFT* Algorithm 2 applied to the same graph, seed sets, and the weight functions* w_0 *and* w_1 *(on* $\mathcal{A}$*) defined as* $w_0(s, t) = \bar{\omega}(t, s)$ *and* $w_1(s, t) = \bar{\omega}(s, t)$.

An easy proof of Proposition 2 is left to the reader. (We introduce in OIFT* the functions w_i and an explicit path map $\pi[\,]$ to help in our analysis in the next section.)

Now, let

$$X_L := \{\langle s, t \rangle \in \mathcal{A}: L(s) > L(t)\}$$

be the (standard) graph cut associated with the partition $\langle L^{-1}(1), L^{-1}(0) \rangle$ and let us define the functional[2] $F_L: \mathcal{A} \to [0, \infty)$ by putting, for every $\langle s, t \rangle \in \mathcal{A}$,

$$F_L(s, t) := \begin{cases} e^{-\omega(s,t)} & \text{for } \langle s, t \rangle \in X_L, \\ 0 & \text{otherwise.} \end{cases}$$

Then, OIFT* Algorithm 2 minimizes the energy

$$\|F_L\|_\infty := \max\{F_L(s, t): \langle s, t \rangle \in \mathcal{A}\},$$

that is, the L_∞ norm of the functional F_L. This puts OIFT*, which is equivalent to OIFT, within the framework of GGC, see, e.g., [5]. (Recall, that the usual graph-cut minimization, associated with the max-flow/min-cut theorem, is defined as L_1 norm of the functional F_L, defined as $\|F_L\|_1 := \sum_{\langle s,t \rangle \in \mathcal{A}} F_L(s, t)$.)

A detailed example of OIFT* Algorithm 2, based on the weights $\omega(s, t)$ of Fig. 1a, is presented in Fig. 2.

4 OIFT Within General Fuzzy Connectedness Framework

In the previous section, we have seen that OIFT Algorithm 1 belongs to the GGC framework. Here, we will argue that it can be also viewed as belonging to a class of general fuzzy connectedness, GFC, algorithms [9]. This will allow us to deduce that OIFT has the properties that all algorithms in GFC are known to have.

In what follows, for a fixed digraph $\langle \mathcal{N}, \mathcal{A} \rangle$, weight maps w_0 and w_1, and the seed sets $\mathcal{S}_0$ and $\mathcal{S}_1$, define the path costs:

$$\psi_{\min}(\langle v_0, \ldots, v_\ell \rangle) := \min_{1 \leq j \leq \ell} w_{L(v_0)}(v_{j-1}, v_j)$$
$$\psi_{\text{last}}(\langle v_0, \ldots, v_\ell \rangle) := w_{L(v_0)}(v_{\ell-1}, v_\ell)$$

for $\ell > 0$ and

$$\psi_{\text{last}}(\langle v_0 \rangle) := \psi_{\min}(\langle v_0 \rangle) := \begin{cases} \infty & \text{for } v_0 \in \mathcal{S}_0 \cup \mathcal{S}_1, \\ -\infty & \text{otherwise.} \end{cases}$$

The map $\psi_{\min}$ is the standard FC cost [8], while ψ_{last}, explicitly defined in [28] (using symbols $f_{i,\omega}$ and $f_{o,\omega}$), is naturally associated with OIFT.

To place OIFT in the GFC framework, we will first represent OIFT* of Algorithm 2 as MOFS* Algorithm 3, which is a version of MOFS algorithm from [9]. The key result here is the following theorem, which is considerably less clear than Proposition 2, since the conditions in lines 8 and 12 of the algorithms have different forms.

[1] In fact, we can use $h(\omega(s, t))$ in place of $e^{-\omega(s,t)}$ when h is any strictly decreasing function from $\mathbb{R}$ into $[0, \infty)$.

[2] Shortly, $F_L := \bar{\omega} \cdot \chi_{X_L}$, where $\chi_{X_L}: \mathcal{A} \to \{0, 1\}$ is the characteristic function of X_L.

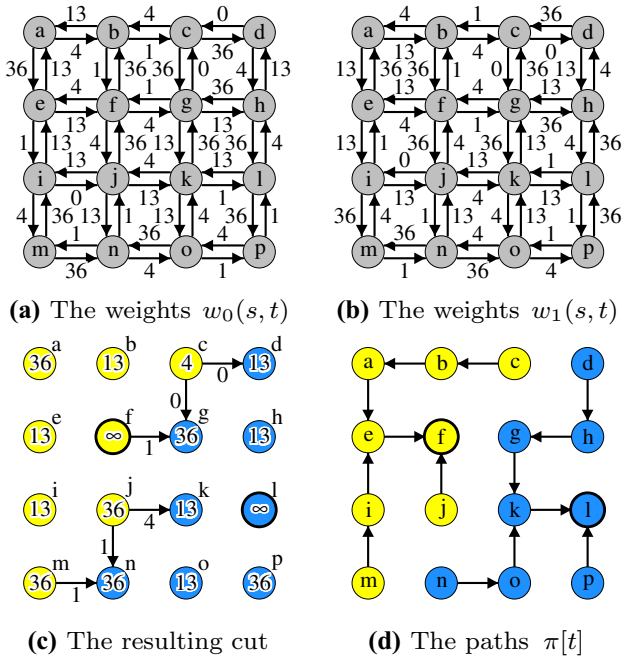

(a) The weights $w_0(s,t)$ **(b)** The weights $w_1(s,t)$

(c) The resulting cut **(d)** The paths $\pi[t]$

Fig. 2 Illustration of OIFT* Algorithm 2. **a**, **b** The weight functions $w_0(s,t) = \bar{\omega}(t,s)$ and $w_1(s,t) = \bar{\omega}(s,t)$, using $\bar{\omega}(s,t) = 100 \cdot e^{-\omega(s,t)}$, truncated to integers for display purposes, where $\omega(s,t)$ are the weights from Fig. 1a. **c** The OIFT* result using the same seeds $\mathcal{S}_0 = \{l\}$ and $\mathcal{S}_1 = \{f\}$ from Fig. 1a, where the node colors blue and yellow indicate the labels $L(t) = 0$ and $L(t) = 1$, respectively, and the values $V(t)$ are indicated inside the nodes. The depicted arcs represent the resulting optimal cut X_L with $\|F_L\|_\infty = e^{-\omega(j,k)} \approx 0.04979$. **d** The computed paths $\pi[t]$ from $\mathcal{S}_{L(t)}$ to t represented in backward, where the arrows indicate the predecessor of each node in the paths. For instance, we have $\pi[p] = \langle l, p\rangle$, $\pi[n] = \langle l, k, o, n\rangle$, $\pi[d] = \langle l, k, g, h, d\rangle$, $\pi[c] = \langle f, e, a, b, c\rangle$, $\pi[j] = \langle f, j\rangle$ and $\pi[m] = \langle f, e, i, m\rangle$ (Color figure online)

Theorem 3 (*OIFT** in GFC format) *Any output of OIFT* Algorithm 2 is identical to that of MOFS* Algorithm 3. In particular, the algorithms MOFS* and OIFT are equivalent.*

Algorithm 3 – MOFS* ALGORITHM

INPUT: Image graph $\langle \mathcal{N}, \mathcal{A}\rangle$, affinities w_0 and w_1, seed sets $\mathcal{S}_0$ and $\mathcal{S}_1$.

OUTPUT: The label map $L: \mathcal{N} \to \{0,1\}$ and an array $\pi[\,]$ such that if $S(t) = 1$, then $\pi[t]$ is a path from $\mathcal{S}_{L(t)}$ to t.

AUXILIARY: An initially empty set Q, variable tmp, the cost function $V: \mathcal{N} \to [-\infty, \infty]$, and a status function $S: \mathcal{N} \to \{0,1\}$, where $S(t) = 1$ for processed nodes and $S(t) = 0$ for unprocessed nodes.

1. **For each** $t \in \mathcal{N}$, **do**
2. Set $S(t) \leftarrow 0$, $V(t) \leftarrow -\infty$, *and* $\pi[t] \leftarrow \langle t\rangle$;
3. **If** $t \in \mathcal{S}_0$, **then**
4. $V(t) \leftarrow \infty$, $L(t) \leftarrow 0$, *and insert* t *in* Q;
5. **If** $t \in \mathcal{S}_1$ **then**
6. $V(t) \leftarrow \infty$, $L(t) \leftarrow 1$, *and insert* t *in* Q.
7. **While** $Q \neq \emptyset$ **do**
8. *Remove from* Q *an* s *in*
$M = \{u \in Q: \psi_{\min}(\pi[u]) = \max_{t \in Q} \psi_{\min}(\pi[t])\}$
such that $V(s) \geq V(u)$ *for all* $u \in M$;
9. Set $S(s) \leftarrow 1$;
10. **For each** $\langle s,t\rangle \in \mathcal{A}$ *such that* $S(t) = 0$ **do**
11. $tmp \leftarrow w_{L(s)}(s,t)$;
12. **If** $\psi_{\min}(\pi[s]\hat{}\,t) > \psi_{\min}(\pi[t])$ *or*
$[\psi_{\min}(\pi[s]\hat{}\,t) = \psi_{\min}(\pi[t])$
and $tmp > V(t)]$ **then**
13. Set $V(t) \leftarrow tmp$, $\pi[t] \leftarrow \pi[s]\hat{}\,t$ *and*
$L(t) \leftarrow L(s)$;
14. **If** $t \notin Q$ **then** *insert* t *in* Q.

We will postpone the proof of Theorem 3 to the end of this section.

Notice that although OIFT* Algorithm 2 has a format of the MOFS algorithm from the GFC framework, it is not precisely of this format. The first difference is that the main GFC algorithm MOFS, when it removes a vertex s from Q, does not have the secondary condition "$V(s) \geq V(u)$ for all $u \in M$" as we have in line 8. But this just means that in MOFS* we are just a bit more precise, when making such choice.

The bigger difference is that MOFS allows some overlaps of the object and background. Specifically, they overlap on the tie zone set TZ defined as the set of all $v \in \mathcal{N}$ for which MOFS, whose output is unique, produces the paths of the same strength from the object and the background. The issue of how to deal with the set TZ is discussed in detail in [9]. In particular, if $w_0(s,t) \neq w_1(u,v)$ for all edges $\langle s,t\rangle$ and $\langle u,v\rangle$, then TZ is empty and the object returned by MOFS* (or OIFT*) is identical to that of MOFS output. Other solutions of the "overlapping problem" are also discussed in [9]. The reader should be warned, however, that a simple minded removal of TZ from the MOSF object (with overlap) may create a set with vertices that are not connected, within the object, to the seeds.

4.1 Proof of Theorem 3

First notice that during the execution of OIFT* Algorithm 2, for any $u \in Q$ either u is a seed or $\pi[u] = \pi[w]\hat{}\,u$ for some $w \in \mathcal{N}$ with $S(w) = 1$.

To prove the theorem, it is enough to show that during the execution of OIFT* Algorithm 2, the condition from line 8 holds, if and only if, the condition from line 8 of MOFS* Algorithm 3 holds, and similarly, for the conditions from line 12.

To see this, we will prove that at any time of the execution of OIFT* Algorithm 2 past line 6 of the code, the following holds for every $u, v \in \mathcal{N}$:

(i) if $S(u) = 1$ and $S(v) = 0$, then $\psi_{\min}(\pi[u]) \geq \psi_{\min}(\pi[v])$;
(ii) if $S(u) = S(v) = 0$ and $V(u) \geq V(v)$, then $\psi_{\min}(\pi[u]) \geq \psi_{\min}(\pi[v])$.

Clearly this holds directly after the execution of line 6. Thus, it is enough to show that these properties are preserved by any consecutive single execution of the while loop, that is, of lines 8–14.

So, fix $u, v \in \mathcal{N}$ for which we will be showing preservation of (i) and (ii). If u is a seed, then after the initialization we have $\psi_{\min}(\pi[u]) = V(u) = \infty$, so (i) and (ii) hold. So, we will assume that u is not a seed. Next, assume that during our execution of lines 8–14 we have taken s from Q.

To see that (ii) is preserved, assume that after the execution of lines 8–14, we have $S(u) = S(v) = 0$. During the execution, the values of either $V(v)$ or $\pi[v]$ can change only in line 13, when $v = t$ for t chosen in line 10 and, during the execution of line 12, we have $w_{L(s)}(s, v) = w_{L(s)}(s, t) = tmp > V(t)$. Hence, the execution of line 13 results with $V(v) = V(t)$ becoming $w_{L(s)}(s, v)$ and $\pi[v] = \pi[t]$ becoming $\pi[s]\hat{}v = \pi[s]\hat{}t$ so that

$$\psi_{\min}(\pi[v]) = \min\{\psi_{\min}(\pi[s]), w_{L(s)}(s, v)\}.$$

The similar analysis holds when either of the values $V(u)$ or $\pi[u]$ is changed during the execution of lines 8–14.

Now, consider 4 cases:

- If none of the values $V(v)$, $\pi[v]$, $V(u)$, or $\pi[u]$ change during the execution of lines 8–14, then clearly (ii) is preserved.
- If, during the execution, we applied the changes in line 13 to both u and v, then $V(u) \geq V(v)$ implies that $w_{L(s)}(s, u) \geq w_{L(s)}(s, v)$ and so,

$$\begin{aligned}\psi_{\min}(\pi[u]) &= \min\{\psi_{\min}(\pi[s]), w_{L(s)}(s, u)\}\\ &\geq \min\{\psi_{\min}(\pi[s]), w_{L(s)}(s, v)\}\\ &= \psi_{\min}(\pi[v])\end{aligned}$$

  giving desired (ii).
- If, during the execution, we applied the changes in line 13 only to u, then $\psi_{\min}(\pi[u]) = \min\{\psi_{\min}(\pi[s]), w_{L(s)}(s, u)\} \geq \psi_{\min}(\pi[s]) \geq \psi_{\min}(\pi[v])$, where the last inequality is implied by $V(s) \geq V(v)$, ensured by the choice of s from Q, and the recursive assumption (ii). Thus, indeed (ii) is preserved.
- Finally, if, during the execution, we applied the changes in line 13 only to v, then $V_{\text{old}}(u) = V_{\text{new}}(u) \geq V_{\text{new}}(v) = w_{L(s)}(s, v)$. Also, since u is not a seed, we have $\pi[u] = \pi[w]\hat{}u$ for some $w \in \mathcal{N}$ with $S(w) = 1$. By (i), used just before we have taken s from Q, we have $\psi_{\min}(\pi[w]) \geq \psi_{\min}(\pi[s])$. Therefore,

$$\begin{aligned}\psi_{\min}(\pi[u]) &= \min\{\psi_{\min}(\pi[w]), V(u)\}\\ &\geq \min\{\psi_{\min}(\pi[s]), w_{L(s)}(s, v)\}\\ &= \psi_{\min}(\pi[v])\end{aligned}$$

  finishing the proof of preservation of (ii).

Next, we will prove preservation of (i). So, assume that after the execution of lines 8–14, we have $S(u) = 1$ and $S(v) = 0$. Then, by (i), used just before we have taken s from Q, we have $\psi_{\min}(\pi[u]) \geq \psi_{\min}(\pi[s])$. Thus, it is enough to show that right after the execution of lines 8–14, we have $\psi_{\min}(\pi[s]) \geq \psi_{\min}(\pi[v])$. This clearly holds if the values $V(v)$ or $\pi[v]$ were not changed. So, assume that they have been changed. Then, as before, we see that

$$\psi_{\min}(\pi[s]) \geq \min\{\psi_{\min}(\pi[s]), w_{L(s)}(s, v)\} = \psi_{\min}(\pi[v])$$

finishing the proof of preservation of (i) and of the theorem.

5 The Local Band Constraint

Let $C\colon \mathcal{N} \to [0, \infty)$ be a fixed vertex cost function associated with an image digraph $G = \langle \mathcal{N}, \mathcal{A} \rangle$. Usually $C(t)$ is defined as a minimum of all possible path-cost functions for the paths from $\mathcal{S}_1$ to t. The path cost can be its geodesic length (i.e., $\psi_{sum}(\langle v_0, \ldots, v_\ell \rangle) := \sum_{1 \leq j \leq \ell} \|v_{j-1} - v_j\|$), as used in geodesic star convexity, but other path costs are also useful. It can also be based on templates of shapes discussed in [4], which will be considered for evaluation in Sect. 6.

The goal of this section is to construct an extension of an edge-weighted digraph $G = \langle \mathcal{N}, \mathcal{A}, \omega \rangle$, discussed above to the edge-weighted digraph $G' = (\mathcal{N}, \mathcal{A}', \omega')$, so that the application of OIFT (Algorithm 1) to G' produces an optimized object satisfying the local band constraint defined below.

To relate local band constraint to boundary band constraint introduced in [13], we first introduce the following notion of *local boundary band* constraint, LBB. In this definition, the symbol $\|\cdot\|$ denotes the standard Euclidean L_2 norm on $\mathcal{N} \subset \mathbb{Z}^2$. The *boundary* of an object $\mathcal{O}$ is defined as

$$\text{bd}(\mathcal{O}) = \{t \in \mathcal{O}\colon \exists s \in \mathcal{A}(t) \text{ such that } s \notin \mathcal{O}\}.$$

Definition 1 (*Local boundary band* (LBB)) For $\Delta, R > 0$ and a cost map $C\colon \mathcal{N} \to [0, \infty)$, a pixel $t \in \mathcal{O}$ is LBB^R_Δ (satisfies local boundary band constraint with band size Δ and parameter R) provided $C(t) < C(s) + \Delta$ for all $s \in \text{bd}(\mathcal{O})$ such that $\|s - t\| \leq R$. An object $\mathcal{O}$ is LBB^R_Δ provided every $t \in \mathcal{O}$ is LBB^R_Δ.

Definition 2 (*Boundary band constraint* (BB)) For $\Delta > 0$, an object $\mathcal{O}$ is BB_Δ (satisfies boundary band constraint with band size Δ) provided it is LBB^∞_Δ, that is, when $C(t) < C(s) + \Delta$ for all $t \in \mathcal{O}$ and $s \in \text{bd}(\mathcal{O})$.

As a consequence of Definition 2, we have that $\text{bd}(\mathcal{O})$ is contained in the band $\{s \in \mathcal{N}\colon C(s) \in (m - \Delta, m]\}$,

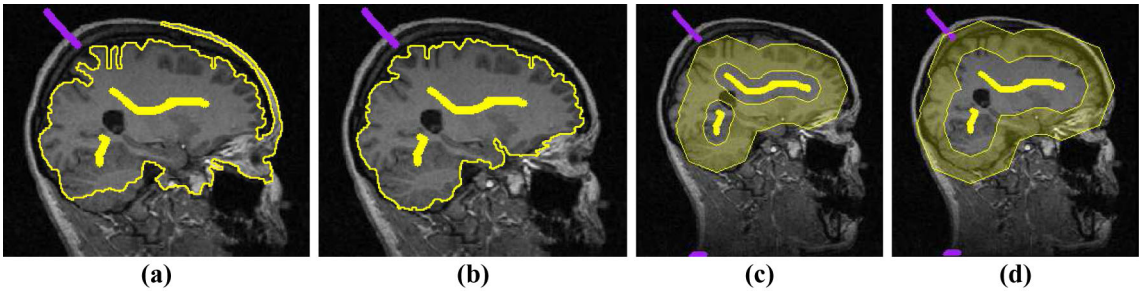

Fig. 3 Brain segmentation example in MRI examination. **a**, **b** Segmentation results by OIFT without and with the BB constraint, respectively. **c**, **d** The BB fixed size band evolves from the seeds, adapting to the image contents. Note that the segmentation boundary achieved in **b** resides within the band area in **d**

where $m = \max\{C(t) : t \in \mathcal{O}\}$. In particular, we have $|C(s) - C(t)| < \Delta$ for all $s, t \in \mathrm{bd}(\mathcal{O})$. Consequently, this regularizes the shape of $\mathrm{bd}(\mathcal{O})$, see [13]. Therefore, the idea of BB is to establish a maximum possible variation of the cost C between the boundary points $\mathrm{bd}(\mathcal{O})$ of the object $\mathcal{O}$ to be segmented. This is expected to prevent the generated segmentation to be irregular in relation to the C-level sets [13]. During the OIFT computation subject to BB, the band changes its reference level set, allowing a better adaptation to the image content, while its width is kept fixed (Fig. 3). Note that this bears some resemblance to narrow band level set [31] and to the regional context of a level line used in [32].

In BB, however, local changes in a part of the object can generate constraint violations in any other part of its boundary, usually resulting in greater sensitivity to the initialization of the cost map C and to the positioning of internal seeds, while in LBB its consistency checks are limited locally, leading to a more flexible solution. Clearly, every BB_Δ object is LBB^R_Δ, but the converse is not true. Nevertheless, for every C and Δ, there exists an $R \in (0, \infty)$ such that the property LBB^R_Δ implies BB_Δ. (This certainly holds for any $R \geq \max\{\|s-t\| : s, t \in \mathcal{N}\}$.) Thus, BB_Δ can be considered as a limit, as $R \to \infty$, of LBB^R_Δ.

In order to facilitate the implementation, we consider an approximate alternative definition, named the *local band constraint* (LB), in order to avoid the continuous analysis of the dynamic set of boundary pixels inside the disks of radius R at runtime, but keeping the main idea of locally restricting the band effects. This effort resulted in the following similar definition.

Definition 3 (*Local band constraint* (LB)) For Δ, $R > 0$ and a cost map $C : \mathcal{N} \to [0, \infty)$, a pixel $t \in \mathcal{O}$ is LB^R_Δ (satisfies local band constraint with band size Δ and parameter R) provided $C(t) < C(s) + \Delta$ for all $s \in \mathcal{N} \backslash \mathcal{O}$ such that $\|s - t\| \leq R$. An object $\mathcal{O}$ is LB^R_Δ provided every $t \in \mathcal{O}$ is LB^R_Δ.

In other words, if $\mathcal{O}$ is LB^R_Δ, then for any pair of pixels s and t such that $\|s - t\| \leq R$ and $C(t) - C(s) \geq \Delta$, we have that $t \in \mathcal{O}$ implies $s \in \mathcal{O}$. Note that neither of the statements "$\mathcal{O}$ is LB^R_Δ" and "$\mathcal{O}$ is LBB^R_Δ" implies the other. Nevertheless, they are closely related, as shown by the following result.

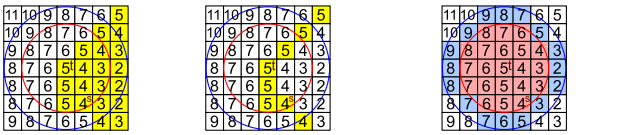

Fig. 4 Example of Proposition 4, where "t is LB^{R+r}_Δ" and "t is $\mathrm{LBB}^R_{\Delta+\delta}$" for $R = 2.5$, $r = 1.0$, $\Delta = 1$, and $\delta = 1$. **a** $\mathcal{O}$, **b** $\mathrm{bd}(\mathcal{O})$, and **c** the disks of radii R and $R + r$

Proposition 4 *Let* $r = \max_{\langle s,t\rangle \in \mathcal{A}} \|s - t\|$ *and* $\delta = \max_{\langle s,t\rangle \in \mathcal{A}} |C(t) - C(s)|$. *If* $\Delta, R > 0$ *and* $\mathcal{O}$ *is* LB^{R+r}_Δ, *then* $\mathcal{O}$ *is* $\mathrm{LBB}^R_{\Delta+\delta}$.

Proof Choose a $t \in \mathcal{O}$. Then $C(t) < C(s) + \Delta$ for all $s \in \mathcal{N} \backslash \mathcal{O}$ such that $\|s - t\| \leq R + r$. We need to show that t is $\mathrm{LBB}^R_{\Delta+\delta}$, that is, that $C(t) < C(u) + \Delta + \delta$ for all $u \in \mathrm{bd}(\mathcal{O})$ such that $\|u - t\| \leq R$. So, take such u. Then, there is an $s \in \mathcal{N} \backslash \mathcal{O}$ with $\langle u, s\rangle \in \mathcal{A}$. Notice that $\|s - t\| \leq \|s - u\| + \|u - t\| \leq r + R$. Using this and the definition of δ, we get $C(t) < C(s) + \Delta \leq C(u) + \Delta + |C(s) - C(u)| \leq C(u) + \Delta + \delta$, as needed. □

Figure 4 illustrates Proposition 4, showing a pixel t that is both LB^{R+r}_Δ and $\mathrm{LBB}^R_{\Delta+\delta}$.

Since usually numbers δ and r are small, the difference should be between the objects with properties LB^R_Δ, LB^{R+r}_Δ, $\mathrm{LBB}^R_{\Delta+\delta}$, or LBB^R_Δ and, for large R, each approximates BB_Δ.

The LB constraint can be implemented, as proposed in Algorithm 4 for OIFT, by considering a modified graph G' with the LB constraint embedded in its arcs. In general, the worst cost should be ∞ for min-sum optimizers (i.e., min-cut/max-flow algorithm) and $-\infty$ for max–min optimizers. In order to maintain a symmetric graph, we also create anti-parallel arcs with the best cutting cost (zero for min-sum and ∞ for max–min optimizers) if they do not exist (line 5 in

Algorithm 4). Note that in G' the set of displacement vectors $D(s) = \{t - s : t \in \mathcal{A}'(s)\}$ varies for different positions of s, leading therefore to a translation-variant adjacency relation.

Algorithm 4 – SEGMENTATION BY OIFT SUBJECT TO THE LB CONSTRAINT

INPUT: Symmetric edge-weighted image digraph $G = \langle \mathcal{N}, \mathcal{A}, \omega \rangle$, non-empty disjoint seed sets $\mathcal{S}_1$ and $\mathcal{S}_0$, cost map $C : \mathcal{N} \to [0, \infty)$, and parameters $R > 0$ and $\Delta > 0$.
OUTPUT: The label map $L : \mathcal{N} \to \{0, 1\}$.
AUXILIARY: Edge-weighted digraph $G' = \langle \mathcal{N}, \mathcal{A}', \omega' \rangle$ with $\mathcal{A} \subset \mathcal{A}'$.

1. *Set* $\mathcal{A}' \leftarrow \mathcal{A}$ *and* $\omega' \leftarrow \omega$.
2. **For each** $\langle s, t \rangle \in \{\langle p, q \rangle \in \mathcal{N} \times \mathcal{N} : \|p - q\| \le R \ \&\ C(p) \ge C(q) + \Delta\}$ **do**
3. | **If** $\langle s, t \rangle \notin \mathcal{A}'$ **then** *Set* $\mathcal{A}' \leftarrow \mathcal{A}' \cup \{\langle s, t \rangle\}$ *and define* $\omega'(s, t) := -\infty$.
4. | **Else** *Redefine* $\omega'(s, t) := -\infty$.
5. | **If** $\langle t, s \rangle \notin \mathcal{A}'$ **then** *Set* $\mathcal{A}' \leftarrow \mathcal{A}' \cup \{\langle t, s \rangle\}$ *and define* $\omega'(t, s) := \infty$.
6. *Compute, by Algorithm 1,* $L : \mathcal{N} \to \{0, 1\}$ *for* G' *and seed sets* $\mathcal{S}_1$ *and* $\mathcal{S}_0$.
7. *Return* L.

Theorem 5 *Let* $G = \langle \mathcal{N}, \mathcal{A}, \omega \rangle$ *be a symmetric edge-weighted image digraph with* $\omega : \mathcal{A} \to \mathbb{R}$. *Let* L *be a segmentation returned by Algorithm 4 applied to* G, *non-empty disjoint seed sets* $\mathcal{S}_1$ *and* $\mathcal{S}_0$, *cost map* $C : \mathcal{N} \to [0, \infty)$, *and parameters* $R > 0$ *and* $\Delta > 0$. *Assume that* $\mathcal{S}_1$ *and* $\mathcal{S}_0$ *are* LB_Δ^R*-consistent, that is, that*

(⋆) there exists a labeling satisfying seeds and LB_Δ^R *constraints.*

Then L *satisfies seeds and* LB_Δ^R *constraints and maximizes the energy* $\varepsilon_{\min}$, *given by (1) w.r.t.* G, *among all segmentations satisfying these constraints.*

Proof In this proof $\varepsilon_{\min}^G$ and $\varepsilon_{\min}^{G'}$ denote the energy $\varepsilon_{\min}$ with respect to G and G', respectively. Let $\mathcal{L} := \{\langle p, q \rangle \in \mathcal{N} \times \mathcal{N} : 0 < \|p - q\| \le R \ \&\ C(p) \ge C(q) + \Delta\}$ and $\mathcal{M} := \{\langle s, t \rangle : (s, t) \in \mathcal{L}\} \backslash \mathcal{A}$. It is easy to see that after the execution of lines 1–5 we have $\mathcal{A}' = \mathcal{A} \cup \mathcal{L} \cup \mathcal{M}$ and

$$\omega'(s, t) = \begin{cases} -\infty & \text{for } \langle s, t \rangle \in \mathcal{L}, \\ \infty & \text{for } \langle s, t \rangle \in \mathcal{M}, \\ \omega(s, t) & \text{otherwise, that is for } \langle s, t \rangle \in \mathcal{A} \backslash \mathcal{L}. \end{cases}$$

Also, by Proposition 1, after the execution of line 6 the labeling L satisfies the seed constraints and maximizes the energy $\varepsilon_{\min}^{G'}$ among all segmentations satisfying seed constraints. We need to show that L satisfies also LB_Δ^R constraints and that it maximizes $\varepsilon_{\min}^G$ among all segmentations satisfying these constraints.

To see this, let $L' : \mathcal{N} \to \{0, 1\}$ be an arbitrary labeling satisfying seeds and LB_Δ^R constraints. It exists by (⋆). Then, by the definition of LB_Δ^R constraints, the set $T' := \{\langle p, q \rangle \in \mathcal{A}' : L'(p) > L'(q)\}$ is disjoint with $\mathcal{L}$. In particular,

$$\begin{aligned} \varepsilon_{\min}^{G'}(L) &\ge \varepsilon_{\min}^{G'}(L') \\ &= \min\{\omega'(s, t) : \langle s, t \rangle \in \mathcal{A}' \ \&\ L'(s) > L'(t)\} \\ &> -\infty. \end{aligned}$$

Hence

$$\begin{aligned} \varepsilon_{\min}^{G'}(L) &= \min\{\omega'(s, t) : \langle s, t \rangle \in \mathcal{A}' \ \&\ L(s) > L(t)\} \\ &> -\infty, \end{aligned}$$

so that the set $T := \{\langle p, q \rangle \in \mathcal{A}' : L(p) > L(q)\}$ must be also disjoint with $\mathcal{L}$. This means that L satisfies LB_Δ^R constraints. To finish the proof we need to show that $\varepsilon_{\min}^G(L) \ge \varepsilon_{\min}^G(L')$. For this notice first that

$$\varepsilon_{\min}^{G'}(L') = \varepsilon_{\min}^G(L'). \tag{2}$$

Indeed, $T' \cup T$ is disjoint with $\mathcal{L}$, so $\langle s, t \rangle \in \mathcal{A}'$ and $L'(s) > L'(t)$ implies that $\langle s, t \rangle \in (\mathcal{A} \backslash \mathcal{L}) \cup \mathcal{M}$. Thus, since $\omega' = \omega$ on $\mathcal{A} \backslash \mathcal{L}$ and $\omega' = \infty$ on $\mathcal{M}$,

$$\begin{aligned} &\varepsilon_{\min}^{G'}(L') \\ &= \min\{\omega'(s, t) : \langle s, t \rangle \in \mathcal{A}' \ \&\ L'(s) > L'(t)\} \end{aligned}$$

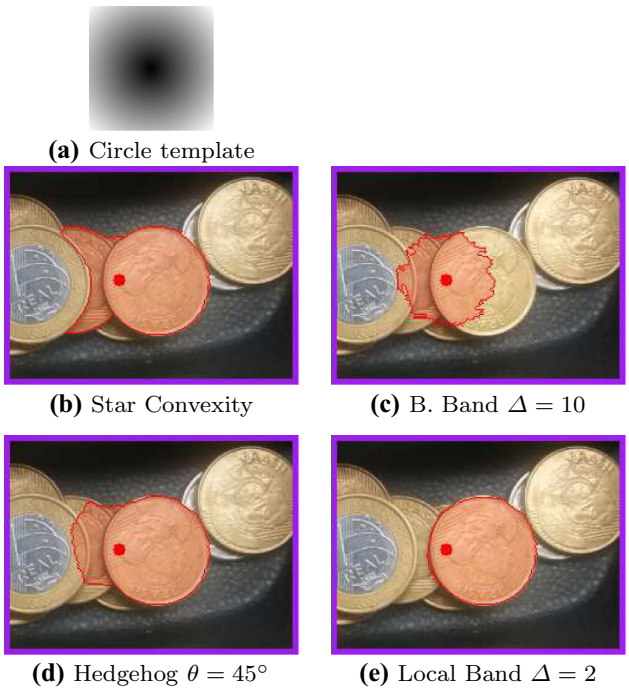

(a) Circle template
(b) Star Convexity
(c) B. Band $\Delta = 10$
(d) Hedgehog $\theta = 45°$
(e) Local Band $\Delta = 2$

Fig. 5 Coin segmentation by OIFT with a circle template in a 250×185 image

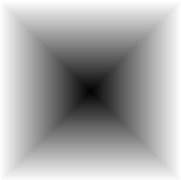

(a) Square template

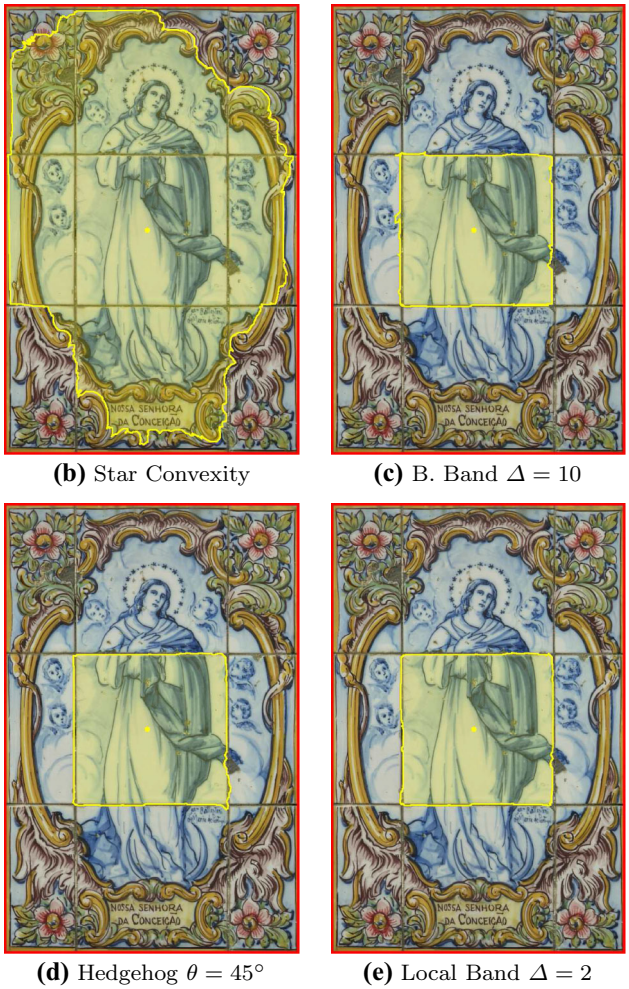

(b) Star Convexity **(c)** B. Band $\Delta = 10$

(d) Hedgehog $\theta = 45°$ **(e)** Local Band $\Delta = 2$

Fig. 6 Wall tile segmentation by OIFT with a square template in a 576×881 image

$$
\begin{aligned}
&= \min\left(\{\omega'(s,t)\colon \langle s,t\rangle \in \mathcal{A}\backslash\mathcal{L}\ \&\ L'(s) > L'(t)\} \cup \{\infty\}\right)\\
&= \min\left(\{\omega(s,t)\colon \langle s,t\rangle \in \mathcal{A}\ \&\ L'(s) > L'(t)\} \cup \{\infty\}\right)\\
&= \varepsilon^{G}_{\min}(L'),
\end{aligned}
$$

as needed. Finally, using (2) for L and L', we obtain

$$\varepsilon^{G}_{\min}(L) = \varepsilon^{G'}_{\min}(L) \geq \varepsilon^{G'}_{\min}(L') = \varepsilon^{G}_{\min}(L'),$$

finishing the proof. □

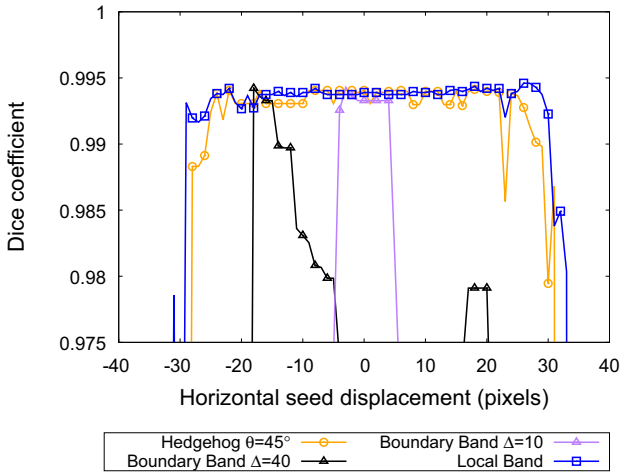

(a) coin

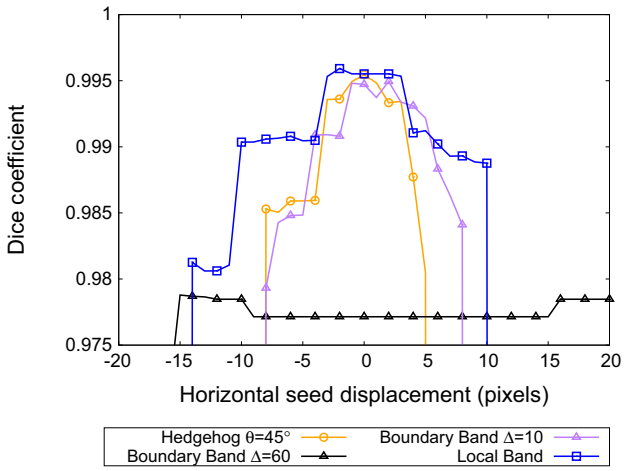

(b) wall tile

Fig. 7 The accuracy curves for different horizontal displacements of the internal seeds

Table 1 The computational time of Algorithm 1 on G', without and with transitive reduction (TR), for the tile segmentation (Fig. 6), for different LB parameters on an Intel Core i3-5005U CPU 2.00 GHz×4 and the percentage gain of using TR

	Time (ms) without TR	Time (ms) with TR	Percent gain
$\Delta = 1, R = 6$	356.2	116.6	67.3%
$\Delta = 1, R = 8$	581.8	175.7	69.8%
$\Delta = 1, R = 10$	886.5	186.8	78.9%
$\Delta = 1, R = 12$	1438.8	218.4	84.8%
$\Delta = 2, R = 6$	329.0	248.6	24.4%
$\Delta = 2, R = 8$	521.2	295.7	43.3%
$\Delta = 2, R = 10$	823.7	340.8	58.6%
$\Delta = 2, R = 12$	1429.7	361.8	74.7%

Table 2 The number of arcs of G', without and with Transitive Reduction (TR), for the tile segmentation (Fig. 6), for different LB parameters and the percentage gain of using TR

	$\|\mathcal{A}'\|$ without TR	$\|\mathcal{A}'\|$ with TR	Percent gain
$\Delta = 1, R = 6$	51,342,944	12,189,774	76.3%
$\Delta = 1, R = 8$	91,391,300	16,260,890	82.2%
$\Delta = 1, R = 10$	149,234,880	20,349,830	86.4%
$\Delta = 1, R = 12$	208,879,992	24,420,058	88.3%
$\Delta = 2, R = 6$	43,204,080	26,245,554	39.3%
$\Delta = 2, R = 8$	79,181,320	34,360,266	56.6%
$\Delta = 2, R = 10$	132,935,960	42,510,658	68.0%
$\Delta = 2, R = 12$	188,510,844	50,623,754	73.1%

6 Experimental Results

In this section, we compare LB with shape constraints commonly employed in graph-based segmentation: geodesic star convexity [19], boundary band [13], and hedgehog shape prior [20,21]. We opted to compare them using max–min optimizers because BB is not yet supported by min-sum optimizers [13].

From the IFT [15] perspective, when the cost map C is the geodesic length (i.e., $\psi_{sum}(\langle v_0, \ldots, v_\ell \rangle) := \sum_{1 \le j \le \ell} \|v_{j-1} - v_j\|$), from $\mathcal{S}_1$ in $G = (\mathcal{N}, \mathcal{A})$, the previous constraints are based on different attributes of a previously computed minimal forest in G rooted at $\mathcal{S}_1$: Geodesic star convexity uses the predecessor map [29], BB and LB constraints exploit the cost map directly, and Hedgehog uses the gradient of the cost map as vector field.

Figure 5 shows the segmentation results by OIFT using different methods, $\omega(s,t) = \|\mathcal{I}(t) - \mathcal{I}(s)\|$ and a circle template, as reference cost map, centered on the center of mass of the internal seeds. The BB constraint fails to give good results compared to local band, due to its greater sensitivity to the template positioning.

Figure 6 shows some results of a tile segmentation using a square template and $\omega(s,t) = \|\mathcal{I}(t) - \mathcal{I}(s)\|$. In order to measure the sensitivity of the most promising methods for different seed positioning, in Fig. 7 we show the accuracy curves using internal seeds in a circular brush of radius 5 pixels with horizontal displacements relative to the object's center and background seeds at the image frame. Note that

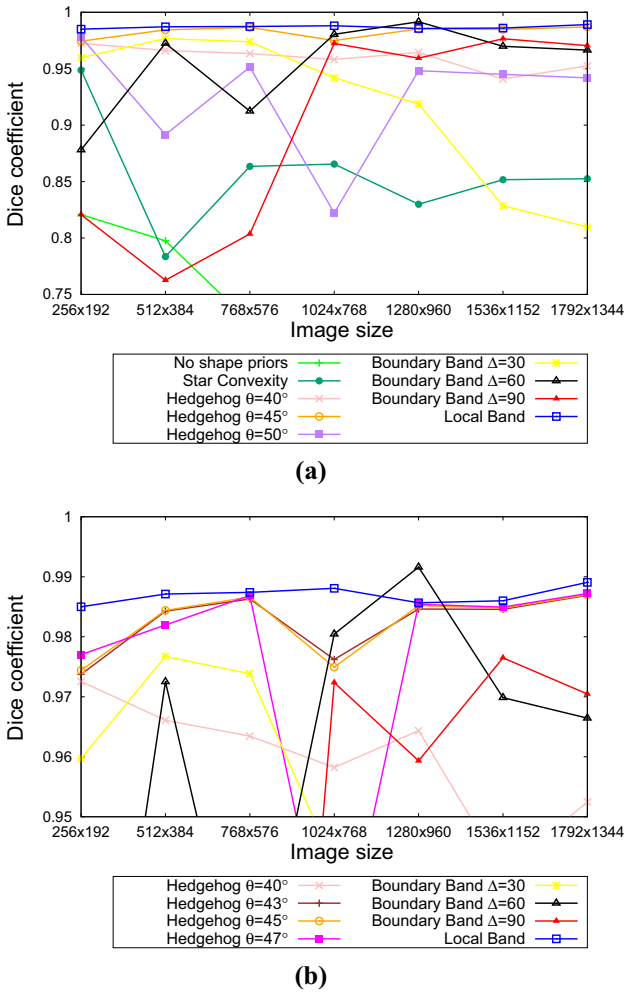

Fig. 9 **a** The mean accuracy values to segment the archaeological fragments for different image resolutions. **b** Zoomed results (accuracy $\ge 95\%$)

for the coin segmentation, LB ($R = 3.5$ and $\Delta = 2$) had slightly more stable results compared to hedgehog, giving almost perfect results for 68.2% of the maximum possible horizontal shift in the coin (radius 44 pixels). BB constraint with $\Delta = 10$ had significantly lower robustness to seed displacements (11.4% of the maximum shift). For higher delta values, BB became unstable. It surprisingly had better results for a left-shifted position to avoid false positives on its right side. For the wall tile segmentation, LB ($R = 3.5$ and $\Delta = 2$) had the most accurate results, giving good results for 10.3%

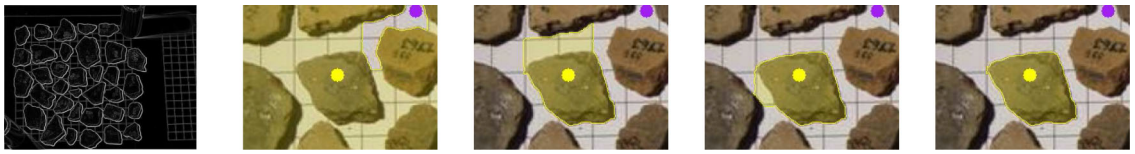

Fig. 8 Archeological fragment segmentation

of the maximum possible horizontal shift in the wall tile (radius 145 pixels). BB constraint with $\Delta = 10$ had worse robustness to seed displacements. For higher values of delta, it was possible to increase its robustness, but at the price of sacrificing its accuracy.

Regarding the computational time, for the tile segmentation (Fig. 6), the max–min optimization on G' with LB ($R = 3.5$ and $\Delta = 2$) took 147.6 ms running on an Intel Core i3-5005U CPU 2.00 GHz×4. In relation to the number of arcs, we have $|\mathcal{A}| \approx 4 \times 10^6$ for G and $|\mathcal{A}'| \approx 12 \times 10^6$ for G' in Algorithm 4. Tables 1 and 2 show the effect of increasing the radius size on the computational time of the max–min optimization on G' and the resulting number of arcs of G', respectively. Note that the computational cost increases considerably for larger radius values, since its computational complexity is $O(|\mathcal{A}'| + |\mathcal{N}| \times K)$, when the finite arc weights are integers in a small interval of size K. The nodes $\mathcal{N}$ and the set of arcs

$$\{\langle p, q\rangle \in \mathcal{A}' : \|p - q\| \leq R \;\&\; C(p) \geq C(q) + \Delta\}$$

from line 2 of Algorithm 4 form a *directed acyclic graph* (DAG). Several of these $-\infty$-valued arcs in ω' that represent the LB constraint may actually be redundant, and we can apply a *transitive reduction* [1] to eliminate them from this DAG. A transitive reduction of a directed graph D is another directed graph with the same vertices and as few arcs as possible, such that if there is a (directed) path from vertex v to vertex w in D, then there is also such a path in the reduction. The transitive reduction of a finite DAG is unique and is a subgraph of the given graph [1].

The redundant arcs from the DAG can be eliminated from $\mathcal{A}'$, as well as their opposite infinite weighted arcs from Line 5 of Algorithm 4. Whenever the cost map C is fixed (e.g., based on a prior template of shapes), the transitive reduction can be computed offline in advance to save computational time. The updated runtime on G' and the cardinality of $\mathcal{A}'$ after removing all redundant arcs are shown in the second columns of Tables 1 and 2 .

We also tested the robustness of the methods in relation to different image resolutions by quantitative experiments, to segment archaeological fragments in seven different resolutions with the geodesic cost. In order to make the experiment more challenging, the simple arc weight $\omega(s,t) = G(s) + G(t)$ was used, disregarding any prior color information, where $G(t)$ denotes the magnitude of Sobel gradient, such that we have several false boundaries (Fig. 8). Figure 9 shows the mean values of the Dice coefficient for segmenting ten fragments for each image resolution, totalizing 70 executions for each method. The overall best results were obtained by LB using $R = 3.5$ and $\Delta = 2$. Hedgehog for different θ values and the same radius presented unstable results (Fig. 8d).

Finally, we conducted experiments with the geodesic cost to segment the liver in medical images of 40 slices of thoracic CT studies of size 512×512, using regular weights $\omega(s,t) = \|\mathcal{I}(t) - \mathcal{I}(s)\|$ and seed sets progressively obtained by eroding the ground truth and its background with twice the radius size (Fig. 10). Although this scenario is apparently advantageous for the BB constraint, in view of the well-distributed and centralized seeds, LB ($R = 3.5$ and $\Delta = 2$) demonstrated good results with the highest accuracy for a large part of the curve (Fig. 11a). We repeated the experiments, but now with the internal seeds shifted by 5 pixels to the left (25% of the maximum possible displacement in the central part of the curves) whenever possible. In this new scenario, the results

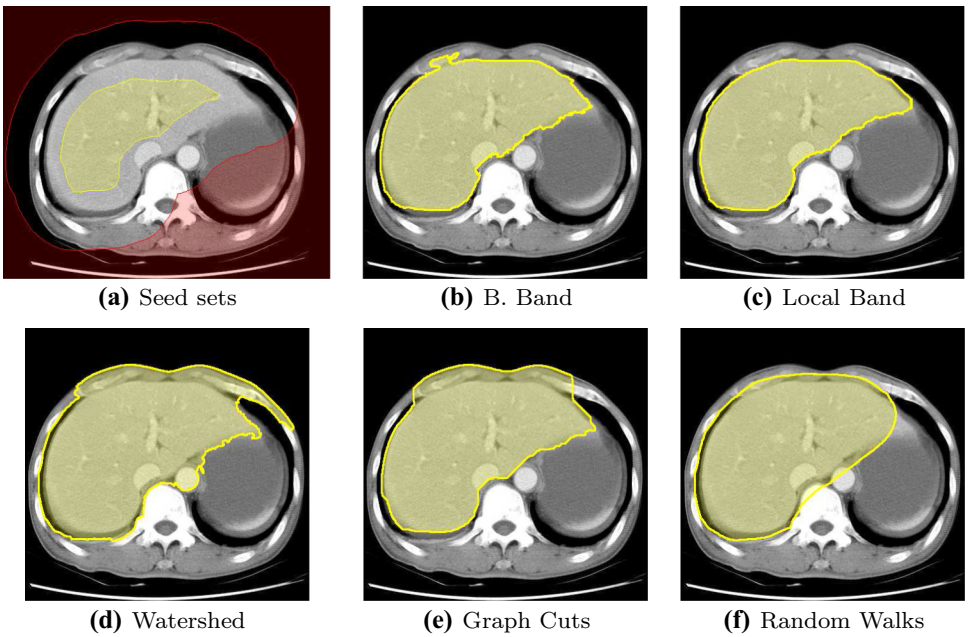

(a) Seed sets **(b)** B. Band **(c)** Local Band

(d) Watershed **(e)** Graph Cuts **(f)** Random Walks

Fig. 10 A thoracic CT image of 512 × 512 pixels. **a** Seed sets obtained by eroding the ground truth of the liver (in yellow) and its background with twice the radius size (in red). **b**, **c** Liver segmentation samples by OIFT subject to different shape constraints. **d**–**f** Segmentation results by classical techniques for the given image graph and seeds (Color figure online)

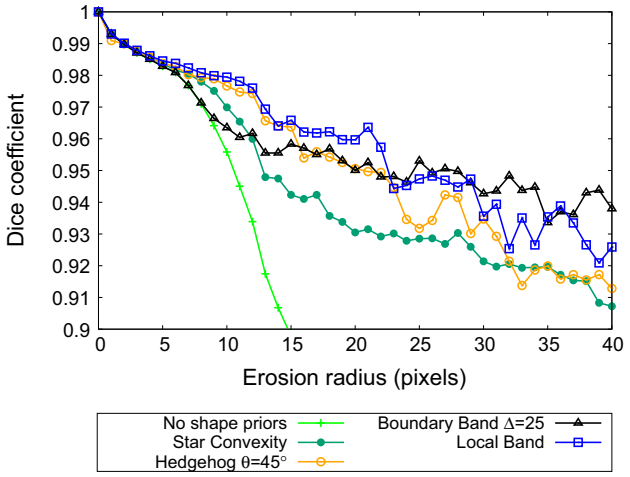

(a) $\mathcal{S}_1$ centralized

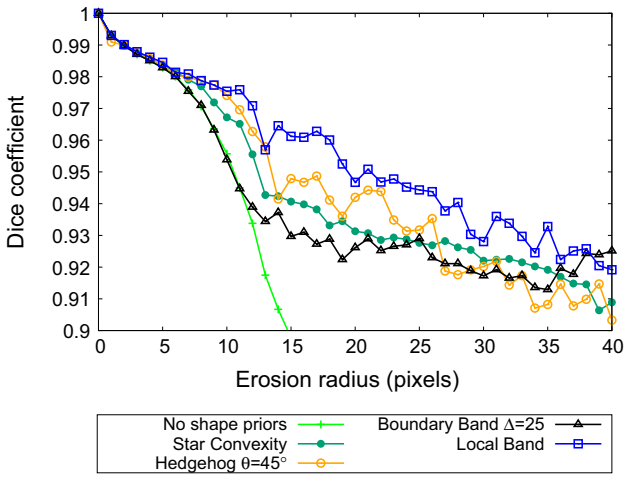

(b) $\mathcal{S}_1$ shifted to the left

Fig. 11 The mean accuracy curves to segment the liver for seed sets obtained by erosion

clearly show that LB is more robust than BB in relation to seed positioning (Fig. 11b). The performance of OIFT with LB is also superior to that revealed by classical techniques for the same image graph G and seeds (Fig. 10d, f).

7 Conclusion

We have proposed the local band shape constraint, which in its limit case (i.e., $R \to \infty$) is strongly related to boundary band constraint and is less sensitive to the seed/template positioning for high-accuracy values. We also demonstrated that OIFT lies in the intersection of the generalized graph cut and the general fuzzy connectedness frameworks, inheriting their properties. To the best of our knowledge, we are also the first to report OIFT with the hedgehog shape prior. As future work, we intend to incorporate the LB constraint into the layers of a hierarchical layered digraph [22] to perform multi-object segmentation and to test LB in 3D medical applications.

Compliance with ethical standards

Conflict of interest The authors declare that they have no conflict of interest.

References

1. Aho, A.V., Garey, M.R., Ullman, J.D.: The transitive reduction of a directed graph. SIAM J. Comput. **1**(2), 131–137 (1972)
2. Bejar, H.H.C., Miranda, P.A.V.: Oriented relative fuzzy connectedness: theory, algorithms, and its applications in hybrid image segmentation methods. EURASIP J. Image Video Process. 2015(21) Jul (2015)
3. Boykov, Y., Funka-Lea, G.: Graph cuts and efficient N–D image segmentation. Int. J. Comput. Vis. **70**(2), 109–131 (2006)
4. de Moraes Braz, C.: Segmentação de imagens pela transformada imagem-floresta com faixa de restrição geodésica. Master's thesis, Instituto de Matemática e Estatística, Universidade de São Paulo, São Paulo, Brasil (2016)
5. Ciesielski, K.C., Udupa, J.K., Falcão, A.X., Miranda, P.A.V.: Fuzzy connectedness image segmentation in graph cut formulation: a linear-time algorithm and a comparative analysis. J. Math. Imaging Vis. **44**(3), 375–398 (2012)
6. Ciesielski, K.C., Udupa, J.K., Falcão, A.X., Miranda, P.A.V.: A unifying graph-cut image segmentation framework: algorithms it encompasses and equivalences among them. In: Proceedings of SPIE on Medical Imaging: Image Processing, vol. 8314 (2012)
7. Ciesielski, K.C., Udupa, J.K., Saha, P.K., Zhuge, Y.: Iterative relative fuzzy connectedness for multiple objects with multiple seeds. Comput. Vis. Image Underst. **107**(3), 160–182 (2007)
8. Ciesielski, K.C., Falcão, A.X., Miranda, P.A.V.: Path-value functions for which Dijkstra's algorithm returns optimal mapping. J. Math. Imaging Vis. **60**(7), 1025–1036 (2018)
9. Ciesielski, K.C., Herman, G.T., Yung Kong, T.: General theory of fuzzy connectedness segmentations. J. Math. Imaging Vis. **55**(3), 304–342 (2016)
10. Ciesielski, K.C., Strand, R., Malmberg, F., Saha, P.K.: Efficient algorithm for finding the exact minimum barrier distance. Comput. Vis. Image Underst. **123**, 53–64 (2014)
11. Cousty, J., Bertrand, G., Najman, L., Couprie, M.: Watershed cuts: thinnings, shortest path forests, and topological watersheds. Trans. Pattern Anal. Mach. Intell. **32**, 925–939 (2010)
12. Cousty, J., Bertrand, G., Najman, L., Couprie, M.: Watershed cuts: minimum spanning forests and the drop of water principle. IEEE Trans. Pattern Anal. Mach. Intell. **31**(8), 1362–1374 (2008)
13. de Moraes Braz, C., Miranda, P.A.V.: Image segmentation by image foresting transform with geodesic band constraints. In: 2014 IEEE International Conference on Image Processing (ICIP), pp. 4333–4337 (2014)
14. de Moraes Braz, C., Miranda, P.A.V., Ciesielski, K.C., Cappabianco, F.A.M.: Graph-based segmentation with local band constraints. In: Couprie, M., Cousty, J., Kenmochi, Y., Mustafa, N. (eds.) Discrete Geometry for Computer Imagery, pp. 155–166. Springer, Cham (2019)
15. Falcão, A.X., Stolfi, J., Lotufo, R.A.: The image foresting transform: theory, algorithms, and applications. IEEE TPAMI **26**(1), 19–29 (2004)

16. Falcão, A.X., Udupa, J.K., Samarasekera, S., Sharma, S., Hirsch, B.E., Lotufo, R.A.: User-steered image segmentation paradigms: live-wire and live-lane. Graph. Models Image Proc. **60**, 233–260 (1998)
17. Freedman, D., Zhang, T.: Interactive graph cut based segmentation with shape priors. In: IEEE Computer Society Conference on Computer Vision and Pattern Recognition, 2005. CVPR 2005, vol. 1, pp. 755–762. IEEE (2005)
18. Grady, L.: Random walks for image segmentation. IEEE Trans. Pattern Anal. Mach. Intell. **28**(11), 1768–1783 (2006)
19. Gulshan, V., Rother, C., Criminisi, A., Blake, A., Zisserman, A.: Geodesic star convexity for interactive image segmentation. In: Proceedings of Computer Vision and Pattern Recognition, pp. 3129–3136 (2010)
20. Isack, H., Veksler, O., Sonka, M.,Boykov, Y.: Hedgehog shape priors for multi-object segmentation. In: 2016 IEEE Conference on Computer Vision and Pattern Recognition (CVPR), pp. 2434–2442 (2016)
21. Isack, H.N., Boykov, Y., Veksler, O.: A-expansion for multiple "hedgehog" shapes. CoRR, arXiv:1602.01006 (2016)
22. Leon, L.M.C., Miranda, P.A.V.D.: Multi-object segmentation by hierarchical layered oriented image foresting transform. In: 2017 30th SIBGRAPI Conference on Graphics, Patterns and Images (SIBGRAPI), pp. 79–86 (2017)
23. Lézoray, O., Grady, L.: Image Processing and Analysis with Graphs: Theory and Practice. CRC Press, California (2012)
24. Li, X., Chen, J., Fan, H.: Interactive image segmentation based on grow cut of two scale graphs. In: Zhang, W., Yang, X., Xu, Z., An, P., Liu, Q., Lu, Y. (eds.) Advances on Digital Television and Wireless Multimedia Communications, pp. 90–95. Springer, Berlin (2012)
25. Madabhushi, A., Udupa, J.K.: Interplay between intensity standardization and inhomogeneity correction in MR image processing. IEEE Trans. Med. Imaging **24**(5), 561–576 (2005)
26. Mansilla, L.A.C., Miranda, P.A.V.: Oriented image foresting transform segmentation: connectivity constraints with adjustable width. In: 29th SIBGRAPI Conference on Graphics, Patterns and Images, pp. 289–296 (2016)
27. Mansilla, L.A.C., Miranda, P.A.V., Cappabianco, F.A.M.: Oriented image foresting transform segmentation with connectivity constraints. In: 2016 IEEE International Conference on Image Processing (ICIP), pp. 2554–2558 (2016)
28. Mansilla, L.A.C., Miranda, P.A.V.: Image segmentation by oriented image foresting transform: handling ties and colored images. In 18th International Conference on Digital Signal Processing, Greece, pp. 1–6 (2013)
29. Mansilla, L.A.C., Miranda, P.A.V.: Image segmentation by oriented image foresting transform with geodesic star convexity. In: 15th International Conference on Computer Analysis of Images and Patterns (CAIP), York, UK, vol. 8047, pp. 572–579 (2013)
30. Miranda, P.A.V., Mansilla, L.A.C.: Oriented image foresting transform segmentation by seed competition. IEEE Trans. Image Process. **23**(1), 389–398 (2014)
31. Sethian, J.A.: A fast marching level set method for monotonically advancing fronts. Proc. Natl. Acad. Sci. USA **93**(4), 1591–5 (1996)
32. Xu, Y., Géraud, T., Najman, L.: Context-based energy estimator: Application to object segmentation on the tree of shapes. In: 2012 19th IEEE International Conference on Image Processing, pp. 1577–1580 (2012)

Caio de Moraes Braz is currently doing a PhD at the Institute of Mathematics and Statistics (IME) of the University of São Paulo (USP), SP, Brazil. He received a B.Sc. in Computer Engineering (2012) and a M.Sc. in Computer Science (2016) from the University of São Paulo (USP), SP, Brazil. His research interests are image processing, data visualization, and computer vision.

Paulo A. V. Miranda is currently professor at the Institute of Mathematics and Statistics (IME) of the University of São Paulo (USP), SP, Brazil. He received a B.Sc. in Computer Engineering (2003) and a M.Sc. in Computer Science (2006) from the University of Campinas (UNICAMP), SP, Brazil. During 2008–2009, he was with the Medical Image Processing Group, Department of Radiology, University of Pennsylvania, Philadelphia, USA, where he worked on image segmentation for his doctorate. He got his doctorate in Computer Science from the University of Campinas (UNICAMP) in 2009. After that he worked as a postdoctoral researcher in a project in conjunction with the professors of the Department of Neurology, UNICAMP. He has experience in computer science, with emphasis on computer vision, image processing, and pattern recognition.

Krzysztof Chris Ciesielski received his masters and PhD degrees in pure mathematics from Warsaw University, Poland, in 1981 and 1985, respectively. He has worked at West Virginia University from 1989 to the present. In addition, since 2006 he has held the position of adjunct professor in the department of radiology at the University of Pennsylvania. He is the author of three books and close to 150 journal research articles. His research interests include both pure mathematics (real analysis, topology, set theory) and applied mathematics (image processing, especially image segmentation). He is an editor of Real Analysis Exchange, the Journal of Applied Analysis, and the Journal of Mathematical Imaging and Vision.

Fábio A. M. Cappabianco is Bachelor of in Computer Engineering from University of Campinas in 2003, M.Sc. in Computer Science from University of Campinas in 2006 (dissertation in computer architectures for image processing, supervisor Guido Araujo), and got his sandwich doctorate in Computer Science from University of Campinas and University of Pennsylvania in 2010 (thesis in MRI of the brain, supervisors Alexandre Falcão and Jayaram Udupa, respectively). He is currently a tenured professor at the Federal University of São Paulo, teaching graduate courses in Computer Science and Biomedical Engineering. He has experience in the area of image processing, biomedical imaging, and computer vision.